Terrestrial environmental change across the onset of the PETM and the associated impact on biomarker proxies: a cautionary tale

Gordon N. Inglis[a,b], Alexander Farnsworth[b,c], Margaret E. Collinson[d], Matthew J. Carmichael[a,b,c], B. David A. Naafs[a,b], Daniel J. Lunt[b,c], Paul J. Valdes[b,c], and Richard D. Pancost[a,b]

[a] Organic Geochemistry Unit, School of Chemistry, and School of Earth Sciences, University of Bristol, Bristol, UK

[b] Cabot Institute, University of Bristol, Bristol, UK

[c] BRIDGE, School of Geographical Sciences, University of Bristol, UK

[d] Department of Earth Sciences, Royal Holloway University of London, UK

Corresponding author: Gordon N. Inglis

Email: gordon.inglis@bristol.ac.uk. Telephone: +44 (0)117 954 6395

Abstract:

The Paleocene-Eocene Thermal Maximum (PETM; ~ 56 million years ago) is the most severe carbon cycle perturbation event of the Cenozoic. Although the PETM is associated with warming in both the surface (up to 8°C) and deep ocean (up to 5°C), there are relatively few terrestrial temperature estimates from the onset of this interval. The associated response of the hydrological cycle during the PETM is also poorly constrained. Here, we use biomarker proxies (informed by models) to reconstruct temperature and hydrological change within the Cobham Lignite (UK) during the latest Paleocene and early PETM. Previous work at this site indicates warm terrestrial temperatures during the very latest Paleocene (ca. 22-26°C). However, biomarker temperature proxies imply cooling during the onset of the PETM (ca. 5-11°C cooling), inconsistent with other local, regional and global evidence. This coincides with an increase in pH (ca. 2 pH units with pH values > 7), enhanced waterlogging, a major reduction in fires and the development of areas of open water within a peatland environment. This profound change in hydrology and environment evidently biases biomarker temperature proxies, including the branched GDGT paleothermometer. This serves as a cautionary tale on the danger of attempting to interpret biomarker proxy records without a wider understanding of their environmental context.

Keywords: lignite, biomarkers, GDGTs, hydrology, Eocene, peat

1. Introduction

The Paleocene-Eocene Thermal Maximum (PETM; ca. 56 million years ago; Ma) is a rapid global warming event associated with the release of ^{13}C-depleted carbon into the ocean-atmosphere system. During the PETM, the deep ocean warmed by ~5°C (Tripati and Elderfield, 2005; Zachos et al., 2008) while sea surface temperatures increased by up to 8°C (Aze et al., 2014; Frieling et al., 2017; Frieling et al., 2014; Schoon et al., 2015; Sluijs et al., 2011; Sluijs et al., 2006; Sluijs et al., 2014; Zachos et al., 2006). During the same interval, continental temperatures increased significantly (ca. 4 to 7°C) (Fricke and Wing, 2004; Gehler et al., 2016; Secord et al., 2010; Wing et al., 2005). There is other evidence for increasing terrestrial temperatures during the PETM, including floral turnover (Schouten et al., 2007; Wing et al., 2005), enhanced insect herbivory (Currano et al., 2008) and mammalian (Secord et al., 2012) and soil faunal dwarfing (Smith et al., 2009). However, our understanding of continental temperature change during the PETM remains restricted to a few, well-sampled regions (primarily western North America), and additional records are required to fully evaluate climate model simulations.

Continental temperatures are also important because they exert a first-order control upon the hydrological cycle. During the PETM, the hydrological cycle broadly exhibits a globally 'wet-wetter, dry-drier' style response (Carmichael et al., 2017). However, there can be significant regional and temporal variability in both proxy and model data. For example, high-latitude and coastal settings are generally characterised by stable and/or increasing rainfall (Carmichael et al., 2017), with proxy evidence for both enhanced terrigenous sediment flux to marginal marine sediments (John et al., 2008) and enhanced chemical weathering (Dickson et al., 2015; Ravizza et al., 2001). In contrast, mid-to-low latitude and continental interior settings are

typically characterised by decreasing rainfall (Carmichael et al., 2017) but an increase in extreme precipitation rates (Carmichael et al., 2018; Handley et al., 2012; Schmitz and Pujalte, 2007). Perturbations to the hydrological cycle also impacted vegetation patterns (Collinson et al., 2009; Jaramillo et al., 2010) and various biogeochemical cycles (e.g. methane cycling; Pancost et al., 2007), potentially playing an important role in maintaining the warmth of the PETM (Zachos et al., 2008) and in the subsequent recovery phase (Gutjahr et al., 2017).

To reconstruct temperature and hydrological change during the PETM, we investigate the biomarker distributions within an immature lignite seam from Cobham, Kent, UK (~48°N palaeolatitude). The Cobham Lignite Bed is inferred to represent an ancient continental mire system and is characterised by a negative carbon isotope excursion characteristic at the PETM onset (Collinson et al., 2003; Pancost et al., 2007; see Collinson et al., 2009 for details on age model). We consider our new results in the context of previously published indicators of vegetation and hydrological change (Collinson et al., 2003; Steart et al., 2007; Collinson et al., 2009; Collinson et al., 2013) and new climate model simulations to develop a holistic and nuanced understanding of paleoenvironmental change in northern Europe across the onset and during the early PETM. Our results refine the understanding of environmental change at this site and serve as a cautionary tale on interpreting biomarker proxies without a wider understanding of their environmental context.

2. Methods

2.1. Sample site

The Cobham Lignite Bed was deposited in a low-lying freshwater setting very near sea-level (~48 °N palaeolatitude). The Cobham Lignite Bed is underlain by a sand and mud unit (shallow marine; S&M). It comprises a thin clay layer (<10 cm) at the base, overlain, in succession, by a charcoal-rich lower laminated lignite (ca. 43 cm thick; lower LL), a charcoal-poor upper laminated lignite (ca. 2 cm thick; upper LL), a middle clay layer (MCL < 10 cm thick) and a charcoal-poor blocky lignite (ca. 130 cm thick; BL). The Woolwich Shell Beds (marginal marine/lagoonal, containing the *Apectodinium* acme; WSB) overly the Cobham Lignite (Collinson et. al. 2009).

2.1.1. Age control

The Cobham Lignite Bed is underlain by the Upnor Formation, which at a nearby site is dated as latest Palaeocene by means of the occurrence of calcareous nannoplankton zone NP9 and magnetochron C25n in its lower part (Collinson et al., 2009). A negative carbon isotope excursion (CIE) of ~ 1.5 ‰ is present near the top of the charcoal-poor upper laminated lignite (54.45 cm), slightly below the middle clay layer. This is interpreted as being the negative CIE characteristic of the PETM (Collinson et al., 2003; 2007; 2009). As such, we interpret the uppermost laminated lignite (54.45 to 57.6cm), middle clay layer (57.6 to 65.3 cm) and blocky lignite (65.3 to 194.8 cm) to reflect PETM age. Based on peat to lignite compaction ratios, the blocky lignite (65.3 to 194.8 cm) is likely to have accumulated as peat during 4–12 kyr (range 1–42 kyr) (Collinson et al., 2009) and thus represents only the early part of the PETM. The shallow-marine Woolwich Formation, which overlies the Cobham Lignite Bed at Cobham, contains the *Apectodinium* acme indicating that it is also within the PETM. For a full description of the stratigraphy, see Collinson et al. (2009).

2.2. Organic Geochemistry

The current study utilised aliquots of total lipid extract (TLE) originally prepared by Pancost et al. (2007) and which had been stored dry and frozen (-20 °C). We focus here exclusively on the lignite sediments (see Supplementary Information). Briefly, the powdered samples were extracted by sonication with a sequence of increasingly polar solvents (four times with dichloromethane (DCM), four times with DCM/methanol (MeOH) (1:1, *v/v),* and three times with MeOH). The total lipid extracts were separated into three fractions using a column packed with (activated) alumina by elution with hexane (apolar fraction), hexane/DCM (9:1 v/v), and DCM/MeOH (1:2 v/v; polar fraction). The polar fraction, containing the GDGTs, was dissolved in hexane/*iso*-propanol (99:1, v/v) and passed through a 0.45 µm PTFE filter.

Apolar fractions were analysed using a Thermoquest Finnigan Trace GC interfaced to a Thermoquest Finnigan Trace MS. This was achieved using a fused silica capillary column (50 m × 0.32 mm) coated with CP-Sil-5 (film thickness 0.12 µm) and via the following temperature programme: 40 °C to 140 °C at 20 °C min^{-1}, then to 300 °C at 4 °C min^{-1}, maintained at 300 °C for 22 min. Polar fractions were analysed by high performance liquid chromatography/atmospheric pressure chemical ionisation – mass spectrometry (HPLC/APCI-MS). Samples were analysed following Hopmans et al. (2016). Normal phase separation was achieved using two Waters Acquity UPLC BEH Hilic columns (2.1 x 150 mm; 1.7 µm i.d.) with a flow rate of 0.2 ml min^{-1}. Samples were eluted isocratically with 78% A and 18% B for 25 min followed by a linear gradient to 35% B over 25 minutes, then a linear gradient to 100% B in 30 minutes, where A = hexane and B = hexane:IPA (9:1, v/v) (Hopmans et al., 2016). Injection volume was 15 µL, typically from 100 µL. Analyses were

145 performed using selective ion monitoring mode (SIM) to increase sensitivity and
146 reproducibility (*m/z* 1302, 1300, 1298, 1296, 1294, 1292, 1050, 1048, 1046, 1036,
147 1034, 1032, 1022, 1020, 1018, 744, and 653).

148

149 *2.3. Biomarker proxies*

150 *2.3.1. Biomarker-based temperature proxies*

151 Branched glycerol dialkyl glycerol tetraethers (brGDGTs) are membrane lipids
152 produced by Bacteria (likely Acidobacteria; Sinninghe Damsté et al., 2018). The
153 distribution of brGDGTs in peats is influenced by mean annual near-surface air
154 temperature (MAAT), with the degree of methylation decreasing as temperature
155 increases (Weijers et al., 2007; Naafs et al., 2017). This is represented by the
156 methylation of branched tetraether (MBT'_{5ME}) index (De Jonge et al., 2014):

157 (1) $MBT'_{5ME} = (Ia + Ib + Ic)/(Ia + Ib + Ic + IIa + IIb + IIc + IIIa)$

158 For application to peats and lignites, MBT'_{5ME} is translated to MAAT using the peat-
159 specific calibration (Naafs et al., 2017):

160 (2) $MAAT_{peat} = 52.18 * MBT'_{5ME} - 23.05$ ($n = 96$, $r^2 = 0.76$; RMSE = 4.7°C)

161 Roman numerals refer to individual GDGT structures shown in the Supplementary
162 Information (Figure S1). In brief, I, II and III represent the tetra-, penta- and
163 hexamethylated components, respectively, and a, b and c represent the brGDGTs
164 bearing 0, 1 or 2 cyclopentane moieties. Penta- and hexamethylated brGDGTs can be
165 methylated at the C-5 position or C-6 position on the alkyl chain. The latter are
166 indicated by an apostrophe (e.g. IIa' – see equation (8)). Note that samples from the

lower laminated lignite (i.e. pre-PETM; n = 7) were previously analysed for branched GDGTs. For more details, see Naafs et al., (2018b).

We also calculate the degree of methylation of brGDGTs with no cyclopentane moieties. This is represented in the $MBT_{acyclic}$ index (Naafs et al., 2018a):

(3) $MBT_{acyclic}$ = (Ia) / ([Ia] + [IIa] + [IIa'] + [IIIa] + [IIIa'])

Recent work has demonstrated that the distribution of bacterial-derived branched glycerol monoalkyl glycerol tetraethers (brGMGTs) in peat can also be influenced by MAAT, with the degree of methylation decreasing as temperature increases (Naafs et al., 2018a). This is represented in the H-$MBT_{acyclic}$ index:

(4) H-$MBT_{acyclic}$ = (H-Ia) / ([H-Ia] + [H-IIa] + [H-IIIa])

In addition to brGDGTs and brGMGTs produced by Bacteria, peats also contain a wide variety of isoprenoidal (iso)GDGTs, produced by Archaea (Weijers et al., 2004). Of these compounds, isoGDGT-5 occurs exclusively within acidic (pH < 5.1) tropical (> 19°C) peats (Naafs et al., 2018b). The relative abundance of isoGDGT-5 is represented using the following index:

(5) %GDGT-5 = (isoGDGT-5)/(isoGDGT-1 + isoGDGT-2 + isoGDGT-3 + isoGDGT-5)

%GDGT-5 values > 1% are only found in peats with both a MAAT > 19.5°C and pH < 5.1. isoGDGT-4 is excluded from this ratio due to co-elution with crenarchaeol. Note that samples from the lower laminated lignite (i.e. pre-PETM; n = 7) were previously analysed for isoGDGT-5. For more details, see Naafs et al., (2018b).

2.3.2. Biomarker-based pH proxies

In addition to temperature, the distribution of brGDGTs can also be influenced by other environmental parameters, such as pH. For instance, both 5- and 6-methyl brGDGTs are more abundant at higher pH (De Jonge et al., 2014). This is represented by a modified version of the cyclisation of branched tetraether (CBT) index (Naafs et al., 2017):

(6) $CBT_{peat} = \log(Ib + IIa' + IIb + IIb' + IIIa')/(Ia + IIa + IIIa)$

CBT_{peat} is translated to peat pH using the following equation (Naafs et al., 2017):

(7) $pH = 2.49 * CBT_{peat} + 8.07$ ($n = 51$; $r^2 = 0.58$; RMSE = 0.8)

6-methyl brGDGTs are also more abundant at higher pH (De Jonge et al., 2014; Yang et al., 2015), represented by the $IR6_{ME}$ index (Yang et al., 2015):

(8) $IR6_{ME} = (IIa' + IIb' + IIc' + IIIa' + IIIb' + IIIc') / (IIa + IIa' + IIb + IIb' + IIc + IIc' + IIIa + IIIa' + IIIb + IIIb' + IIIc + IIIc')$

Peat pH can also be reconstructed using the isomerisation of bacterial-derived hopanoids (C_{31} hopane ββ/(ββ+αβ; Pancost et al., 2003). This index is translated to pH using the following equation (Inglis et al., 2018):

(9) $pH = 5.22 * (C_{31}$ hopane ββ/(ββ+αβ) + 3.11 ($n = 94$, $r^2 = 0.64$; RMSE = 1.4)

2.4. Modelling simulations

Temperature and precipitation estimates were obtained for the Early Eocene (Ypresian) from an ensemble of coupled atmosphere–ocean GCMs. These simulations include the EoMIP ensemble (Lunt et al., 2012), but also more recent simulations (Inglis et al., 2017; Kiehl and Shields, 2013; Sagoo et al., 2013) (Table 1).

We also generate new temperature and precipitation estimates using a revised version of HadCM3L, HadCM3L-I2 (Table 1). Using the nomenclature of Valdes et al. (2017) these new model simulations are carried out using the HadCM3L-M2.1aD version of the model. The boundary conditions (paleogeography, solar forcing, orbit) representing the Ypresian are the same as in Lunt et al. (2016) but with modifications made to the ozone distribution such that it more closely reproduces modern ozone and consequently surface air temperature values when run under modern conditions. A dynamic vegetation model, TRIFFID (Top-down Representation of Interactive Foliage and Flora Including Dynamics; Cox, et al. 1998), was utilized alongside the MOSES 2.1 land surface scheme (Cox, et al. 1999). This allows a stage specific, realistic represenation of vegetation patterns and feedbacks on the climate system. These new simulations were initialised from a previous fully equilibriated (10,422 model years), 2x preindustrial CO_2 run of the Ypresian (Farnsworth et al., 2019). One simulation was kept constant at 2x preindustrial CO_2 for 1,000 model years, while the second experiment used 6x preindustrial CO_2 for 1,000 model years. A mean of the last 50 years is used to produce the reported climatologies from both simulations. To study changes in the occurrence of extreme events, we also include the simulations by Carmichael et al. (2018) (HadCM3L-C; Table 1). Those simulations are performed with atmospheric CO_2 at 2*x* and 4*x* preindustrial concentrations. However, unlike other HadCM3L simulations, precipitation rates were recorded at every model hour for the 99-year run. Within the simulated palaeogeography, the nearest land point to the Cobham locality was identified using the Getech Plc. plate model at the mid-point of the appropriate geological stage (mid-Ypresian), which is consistent with the paleogeographies used in HadCM3L-I and HadCM3L-V simulations.

Simulation	CO_2 (relative to pre-industrial)	Reference
HadCM3L	x2, x4, x6	Lunt et al. (2012)
HadCM3L-I	x2, x4	Inglis et al. (2017)
HadCM3L-I2	x2, x6	*This paper*
HadCM3L-C	x2, x4	Carmichael et al., (2018)
HadCM3L-V	x6	Inglis et al. (2017)
ECHAM	x2	Heinemann et al. (2009)
CCSM3W	x4, x8, x16	Winguth et al. (2010; 2012)
CCSM3H	x2, x4, x8, x16	Huber and Caballero (2011)
CCSM3K	x5	Kiehl and Shields (2013)
GISS	x4, x8, x16	Roberts et al. (2009)
FAMOUS-1	x2	Sagoo et al. (2013)
FAMOUS-2	x2	Sagoo et al. (2013)

Table 1: Summary of model simulations. See the supplementary information and original references for more details

3. Results

3.1. Biomarker distributions in Cobham lignite sediments

The branched GDGT (brGDGT) distribution within the lower laminated lignite (4.65 to 43.3 cm) is dominated by tetramethylated brGDGTs (average: 90% of the total brGDGT assemblage; Fig. 1a). Within the upper laminated lignite (54.15 to 55.9 cm), the relative abundance of tetramethylated brGDGTs decreases (average: 78 % of the total brGDGT assemblage). The relative abundance of tetramethylated brGDGTs decreases further within the blocky lignite (average: 65% of the total brGDGT assemblage; 67.5 to 194.8 cm).

The isoprenoidal GDGT (isoGDGT) distribution within the lower laminated lignite (4.65 to 43.3 cm) is dominated by GDGTs with 0 to 5 cyclopentane moieties, and the abundance of isoGDGT-5 is high (average %GDGT-5: 3.0%). Within the upper laminated lignite (54.15 to 55.9 cm), the abundance of isoGDGT-5 is slightly lower

(average %GDGT-5: 2.3%). Within the blocky lignite (67.5 to 194.8 cm), isoGDGT-5 is typically absent (although there are exceptions; e.g. 121.9cm) and the relative abundance of isoGDGT-0 increases significantly (average: 80% of total isoGDGT assemblage).

The Cobham lignite also contains recently identified branched and isoprenoidal glycerol monoalkyl glycerol tetraethers (brGMGTs and isoGMGTs, respectively; Naafs et al., 2018a). The isoGMGT distribution is dominated by isoGMGT-0 throughout (*m/z* 1300; average: 95 % of the total isoGMGT assemblage). The brGMGT distribution within the lower laminated lignite (4.65 to 43.3 cm) is dominated by brGMGT-Ia (*m/z* 1020; average: 85 % of the total brGMGT assemblage; Fig. 1a). Within the upper laminated lignite (54.15 to 55.9 cm), the relative abundance of brGMGT-Ia decreases (average: 75 % of the total brGMGT assemblage). The relative abundance of brGMGT-Ia decreases further within the blocky lignite (average: 65% of the total brGMGT assemblage; 67.5 to 194.8 cm).

The Cobham lignite also contains a range of bacterial-derived C_{27}–C_{32} hopanes and C_{27}–C_{30} hopenes (see Pancost et al., 2007 for full details). The hopanoid distribution within the lower laminated lignite (4.65 to 43.3 cm) is dominated by the (22R)-17α,21β(H)-homohopane (C_{31}) (average: 31% of total hopanoid assemblage). This is one of the most abundant hopanoids in modern peats and typically dominates the hopane distribution within acidic, ombrotrophic bogs (Inglis et al., 2018). The relative abundance of the (22R)-17α,21β(H)-homohopane (C_{31}) decreases within the upper laminated lignite (average: 15% of total hopanoid assemblage) and the blocky lignite (average: 5% of total hopanoid assemblage).

3.2. MAAT and pH trends in the Cobham Lignite inferred from biomarker proxies

Branched GDGT-derived MAAT estimates from the lower laminated lignite (4.65 to 43.3 cm) are relatively stable and range between ca. 22 and 26 °C (average: 24°C; Naafs et al., 2018b; Fig. 2). Lower MAAT estimates are observed within the upper laminated lignite and blocky lignite. However, see Section 4.1 and 4.2 for further discussion on the validity of these results. CBT_{peat} and C_{31} hopane ββ/(ββ+αβ)-derived pH estimates from the lower laminated lignite (4.65 to 43.3 cm) are relatively low (average: 5.3 and 4.4 pH units, respectively; Fig. 3a-b). Both pH estimates increase slightly in the upper laminated lignite (average: 6.0 and 4.6 pH units, respectively; Fig. 3a-b), and then increase further within the blocky lignite (average: 6.8 and 6.3 pH units, respectively; Fig. 3a-b).

4. Discussion

4.1. Biomarker-derived temperature estimates across the onset of the PETM

Branched GDGT-derived MAAT estimates from the lower laminated lignite pre-PETM interval (i.e. 4.65 to 54.15 cm) indicate warm terrestrial temperatures (ca. 22 to 26°C; average: 24°C; Naafs et al., 2018b; Fig. 2). Naafs et al., (2018b) also identified the occurrence of isoGDGTs with > 5 cyclopentane moieties during the pre-PETM interval, indicating minimum MAAT estimates of 19°C. High $H\text{-}MBT_{acyclic}$ values within the lower laminated lignite (4.65 to 54.15 cm) would also imply elevated terrestrial temperatures (Naafs et al., 2018a). Our biomarker-based temperature estimates agree with MAAT estimates for the Cobham region simulated by climate model simulations run at high CO_2 concentrations (e.g. CCSM3-H 8x and 16x PI; CCSM3-W 16x PI; Figure 4a; Table 1). They also agree with climate model simulations which have modified specific model parameters (e.g. CCSM3-K 5x PI, HadCM3L-V 6x PI, FAMOUS-1 2x

PI; Figure 4a). The latter are in close agreement with existing proxy-based CO_2 estimates for the PETM (Hollis et al., 2019).

Branched GDGT-derived MAAT estimates decrease within the PETM-aged upper laminated lignite (54.45 to 55.9 cm) and blocky lignite (67.5 to 194.8 cm), indicating lower terrestrial temperatures at the onset and during the early PETM (ca. 11 to 20°C; average: 15°C; Fig. 2). The PETM-aged blocky lignite (67.5 to 194.8 cm) also contains a lower abundance of isoGDGT-5 (Fig. 2d; but see pH discussion below; section 4.2.3) and lower H-$MBT_{acyclic}$ values (Fig. 2c), both suggesting lower temperatures. Although the absolute temperature estimates agree with MAAT estimates for this region derived from climate model simulations run at lower CO_2 concentrations (e.g. HadCM3L 2x and 4x PI; ECHAM 2x PI; CCSM3-H 2x and 4x PI, GISS 4x PI; Figure 4a) or that have modified specific model parameters (e.g. HadCM3L-I2 x2 and x6 PI; FAMOUS-2 x2 PI; Figure 4a), for all model simulations in our ensemble with more than one CO_2 concentration (Table 1; Supplementary Information), there is warming at the Cobham location as CO_2 increases.

Decreasing terrestrial temperatures in the upper laminated lignite and the blocky lignite are inconsistent with the presence of the *Apectodinium* acme throughout the overlying Woolwich Shell Beds and the short accumulation time estimated for the BL, both of which suggest that the blocky lignite accumulated as peat during the early part of the PETM (Collinson et al 2009). Lower temperatures are also inconsistent with increasing palm pollen in some BL samples (Collinson et al., 2009). Decreasing temperatures are also at odds with the regional response, with proxy evidence for increasing terrestrial temperatures in northern Europe during the PETM (up to 6°C; Schoon et al., 2015). The marine realm also indicates increasing temperatures in northern Europe during the PETM, with evidence for 3 to 4°C of surface ocean

warming in both the Bay of Biscay (Bornemann et al., 2014) and the North Sea (Schoon et al., 2015). Decreasing terrestrial temperatures also differ from the global response during the PETM (Hollis et al., 2019; Jones et al., 2013; McInerney and Wing, 2011). Collectively, this implies that the biomarker-based paleotemperature proxies in the upper laminated lignite and blocky lignite are impacted by non-thermal influences or ecological signals; below we explore what these controls could be.

4.2. Exploring additional controls upon peat-specific biomarker temperature proxies

4.2.1. Vegetation

The lower laminated lignite (pre-PETM) is dominated by fern spores and is rich in charcoal, including fern leaf stalks, all of which were interpreted to indicate a fire-prone, low-diversity vegetation (Collinson et al., 2009). In contrast, the upper laminated lignite and blocky lignite (PETM) are characterised by the reduction then loss of ferns and charcoal, an increase in wetland plants (including cupressaceous conifers) and a more varied flowering plant community with palms and eudicots. Although it has been previously argued that changes in vegetation could have influenced the distribution of brGDGTs in peatlands (e.g. Weijers et al., 2011), this was later attributed to the overly strong pH correction on the MBT/CBT proxy (Inglis et al., 2017). Indeed, recent studies within modern peatlands (Naafs et al., 2017; Naafs et al., 2019) and ancient lignites (Inglis et al., 2017) have indicated that vegetation change is less of a concern than originally inferred by Weijers et al. (2011). As such, we argue that, although there is vegetation change, it is unlikely to have exerted a primary control upon biomarker paleotemperature proxies in the Cobham Lignite.

348 4.2.2. Lithofacies

349 The Cobham Lignite Bed is characterised by two different lithofacies (laminated vs
350 blocky lignite). The laminated lignite is characterised by repeated (episodic) deposition
351 of charcoal (mostly from local sources, via run-off related local transport; Steart et al.,
352 2007), whereas the overlying blocky lignite is dominated by continuous deposition of
353 non-woody material in a persistent peat-forming environment (Steart et al., 2007).
354 Whilst previous studies have noted subtle differences in brGDGT distributions (and
355 therefore, MAAT estimates; up to 4°C) between different lithofacies (e.g. lignite vs
356 shallow marine sediments; Inglis et al., 2017), a decline in biomarker-based
357 temperature estimates within the Cobham Lignite Bed occurs within the upper
358 laminated lignite (54 to 56 cm; Figure 2) and prior to changes in lithofacies. Therefore,
359 lithofacies are not a primary control upon biomarker paleotemperature proxies in the
360 Cobham Lignite.

361

362 4.2.3. pH, hydrology and presence of open water areas

363 Within the Cobham Lignite Bed, we reconstruct pH using two independent, peat-
364 specific pH proxies: 1) CBT_{peat}, based upon the cyclisation of brGDGTs (Naafs et al.,
365 2017), and 2) the C_{31} hopane ββ/(αβ+ββ) index, based upon the isomerisation of C_{31}
366 hopanes (Inglis et al., 2018). Within the lower laminated lignite (pre-PETM), brGDGT-
367 and hopanoid-derived pH estimates (pH: ca. 4 to 5.5) are low and indicate acidic
368 conditions (Fig. 3). The occurrence of isoGDGT-5 (> 1%; Fig. 2d), the absence of 6-
369 methyl brGDGTs (IR_{6ME} < 0.01; Fig. 3c) and the dominance of the C_{31} αβ hopane
370 provides additional evidence for acidic conditions within the lower laminated lignite.
371 We observe a remarkable increase in hopanoid- and brGDGT-derived pH estimates

within the upper laminated lignite (0.5 pH unit) and especially the blocky lignite (ca. 2 pH units to pH values > 7.5; Fig. 3). The upper laminated lignite and blocky lignite also contain a higher abundance of pH-sensitive 6-methyl brGDGTs (average IR_{6ME}: 0.23 and 0.29, respectively; Fig. 3) and a lower abundance of the C_{31} αβ hopane. This indicates a profound change in the environment during the onset and early PETM and provides an alternative explanation for the decrease in the abundance of isoGDGT-5 (see 4.1; Naafs et al., 2018b).

An increase in pH values within the onset and early PETM implies changes in local hydrology, supported by other hydrological and botanical indicators at Cobham (UK), including those discussed above. In addition, the blocky lignite is characterised by an increased percentage of *Inaperturopollenites* pollen (representing swamp-dwelling cupressaceous conifers) and *Sparganiaceaepollenites* pollen (representing marginal aquatic monocotyledonous angiosperm herbs), indicating the development of waterlogged swamp environments (Collinson et al., 2009). The base of the blocky lignite also includes the unusual co-occurrence of two genera of freshwater, free-floating water plants, the heterosporous ferns *Salvinia* and *Azolla* (Collinson et al., 2013). There is also the loss of wildfires, with both the upper laminated lignite and blocky lignite having a significant reduction in, or loss of, both macroscopic and microscopic charcoal (Collinson et al., 2009).

Taken together, the evidence indicates enhanced waterlogging during the onset of the PETM and the development a persistent peatland with patches of open water. The development of open water conditions is likely to be associated with the input of brGDGTs from aquatic sources (as observed in lakes and ponds; e.g. Colcord et al., 2015; Huguet et al., 2015; Tierney and Russell, 2009; Weber et al., 2018). Aquatic brGDGTs can reflect near-bottom water temperatures (Weber et al., 2018)

and application of mineral soil or peat calibrations in modern lacustrine settings consistently yields colder-than-predicted temperatures (up to 10°C in modern systems; Tierney et al., 2010; Zink et al., 2010). The input of GGDTs from aquatic sources can therefore explain the apparent cooling in our brGDGT-derived temperature estimates during the onset of the PETM. This also indicates that the brGDGT paleothermometer in terrestrial archives should not be employed in settings where major changes in pH and hydrology took place. Future work aiming to determine palaeotemperatures would therefore benefit from accompanying proxy-based pH reconstructions based on the distribution of hopanes (Inglis et al., 2018) or branched glycerol dialkyl glycerol tetraethers (brGDGTs) (Naafs et al., 2017) or alternative palaeohydrological indicators (e.g. *n*-alkane δ^2H values; Sachse et al., 2012).

4.3. A shift towards wetter conditions in northern Europe during the PETM

Our data – as well as previously published proxy evidence – suggest a shift towards wetter conditions during the PETM at Cobham (see section 4.2). To test these observations, we used the same ensemble of model simulations (see section 4.1; Table 1) to investigate changes in mean annual precipitation (MAP) at Cobham (UK) for two PETM-type scenarios (i.e. doubling or tripling of CO_2; Fig. 4b). For a tripling of CO_2, model simulations indicate stable (e.g. HadCM3L) or decreasing MAP (22%; e.g. HadCM3L-I2). For a doubling of CO_2, model simulations indicate increasing (6 to 7 %; CCSM3-H, HadCM3L-C), stable (e.g. HadCM3L) or decreasing MAP (5 to 22%; HadCM3L-I, CCSM3-W). Stable or decreasing MAP is inconsistent with proxy evidence at Cobham. However, model simulations run at hourly resolution (i.e. HadCM3L-C) also show a change in precipitation extremes at Cobham for a doubling of CO_2, with an increase in the 90th percentile storm extreme rate (+7%; HadCM3L-

C). This indicates an increase towards more intense rainfall events. Furthermore, an increase in tail width (+28%) indicates more frequent heavy rainfall events of a given size (Carmichael et al., 2018), which could induce waterlogging events. Decoupling between MAP and extreme events has previously been noted for other mid-latitude PETM settings (e.g. Tunisia; Carmichael et al. 2018) and should be considered in future proxy-model comparisons.

Geochemical and botanical proxies at other sites provide evidence for enhanced rainfall in northern Europe during the PETM, with evidence for an increase in wetland-type environments in northern France (Garel et al., 2013) and other parts of the region surrounding the North Sea (Eldrett et al., 2014; Kender et al., 2012). There is also evidence for abundant low-salinity tolerant dinocysts (Sluijs et al., 2007), enhanced clay mineral deposition (Bornemann et al., 2014) and isotopically-depleted tooth apatite $\delta^{18}O$ values (Myhre et al., 1995) within North Sea marine sediments, all of which indicate wetter conditions during the PETM. This indicates a shift towards wetter conditions in northern Europe during the PETM and perhaps an increase in the occurrence of extreme rainfall events (Carmichael et al., 2018). In these settings, terrestrial biomarker proxies may be subject to additional controls (e.g. pH, hydrology and/or the presence of open water areas) and should therefore be interpreted within a multi-proxy framework.

5. Conclusions

Here we have reconstructed terrestrial paleoenvironmental change within the Cobham Lignite Bed, which spans the very latest Paleocene, onset and early part of the PETM. Proxies indicate high terrestrial temperatures prior to the PETM (22 to 26°C), consistent with model simulations. However, inconsistent with local, regional and

global evidence, the biomarker proxies seem to indicate significant cooling during the onset and early PETM (ca. 5 to 11°C). We attribute this to enhanced waterlogging and the development of a persistent peatland with areas of open water, biasing the brGDGT paleothermometer. This study implies the need for care when applying biomarker-based temperature proxies in highly dynamic terrestrial environments (e.g. lacustrine/mire settings). It also serves as a cautionary tale on the danger of attempting to interpret wetland proxy records without a wider understanding of the environmental context, especially pH and hydrology.

Acknowledgements

This research was funded through the advanced ERC grant 'The Greenhouse Earth System' (T-GRES. Project reference: 340923). RDP also acknowledges the Royal Society Wolfson Research Merit Award and funding from the NERC. BDAN acknowledges additional funding from a Royal Society Tata University Research Fellowship. We thank the NERC Life Sciences Mass Spectrometry Facility (Bristol) for analytical support. A.F., D.J.L. and R.D.P acknowledge funding from NERC through NE/K014757/1, NE/I005722/1, NE/I005714/1, and (PJV also) NE/P013805/1. We gratefully acknowledge funding to M.E.C. from NERC grant NE/J008656/1 and to R.D.P. from NERC grant NE/J008591/1. M.E.C. thanks the Leverhulme Trust for providing funding (Grant number F/07/537/0) and Alfred McAlpine, AMEC and Channel Tunnel Rail Link for access to the Cobham site. Finally, we thank Alan Haywood and two anonymous reviewers for their constructive comments.

Data availability

Data can be accessed via the online supporting information, via http://www.pangaea.de/, or from the author (email: gordon.inglis@bristol.ac.uk).

Figure captions

Figure 1: Fractional abundance of (a) branched GDGT and (b) isoprenoidal GDGT lipids within the lower laminated lignite (pre-PETM), upper laminated lignite (PETM onset) and blocky lignite (early PETM)

Figure 2: Terrestrial biomarker proxies before, across the onset and during the early part of the PETM at Cobham. a) Branched GDGT-implied MAAT estimates obtained via $MAAT_{peat}$ proxy, b) $MBT_{acyclic}$, c) $H\text{-}MBT_{acyclic}$ and d) %GDGT-5. Dashed line corresponds to onset of CIE (54.45 cm). Note that $MAAT_{peat}$ and %GDGT-5 estimates from the charcoal-rich lower laminated lignite (i.e. pre-CIE; n = 7) were published in Naafs et al. (2018).

Figure 3: Peat pH before, across the onset and during the early part of the PETM at Cobham, a) C_{31} hopane (ββ/αβ+ββ)-derived pH estimates, b) CBT_{peat}-derived pH estimates, b c) IR_{6ME} (the ratio between 5- and 6-methyl brGDGTs. High values imply higher pH). Dashed line corresponds to onset of CIE.

Figure 4. Model-derived mean annual surface temperature (a) and mean annual precipitation (b) estimates as a function of CO_2 at Cobham (UK). Simulations represent the mid-point of the most appropriate geological stage (Ypresian; 56 to 47.8 Ma). For full details on each model simulation, see Supplementary Information. (For interpretation of the references to color in this figure legend, the reader is referred to the web version of this article.)

References

Aze, T., Pearson, P.N., Dickson, A.J., Badger, M.P.S., Bown, P.R., Pancost, R.D., Gibbs, S.J., Huber, B.T., Leng, M.J., Coe, A.L., Cohen, A.S. and Foster, G.L. (2014) Extreme warming of tropical waters during the Paleocene–Eocene Thermal Maximum. *Geology*, **42**. 739-742

Bornemann, A., Norris, R.D., Lyman, J.A., D'Haenens, S., Groeneveld, J., Röhl, U., Farley, K.A. and Speijer, R.P. (2014) Persistent environmental change after the Paleocene–Eocene Thermal Maximum in the eastern North Atlantic. *Earth and Planetary Science Letters*, **394**, 70-81.

Carmichael, M.J., Inglis, G.N., Badger, M.P., Naafs, B.D.A., Behrooz, L., Remmelzwaal, S., Monteiro, F.M., Rohrssen, M., Farnsworth, A., Buss, H.L. Dickson, A.J, Valdes, P.J., Lunt, D.J and Pancost, R.D. (2017) Hydrological and associated biogeochemical consequences of rapid global warming during the Paleocene-Eocene Thermal Maximum. *Global and Planetary Change*, **157**,114-138.

Carmichael, M.J., Pancost, R.D. and Lunt, D.J (2018) Changes in the occurrence of extreme precipitation events at the Paleocene–Eocene thermal maximum. *Earth and Planetary Science Letters*. **501**, 24-36.

Colcord, D.E., Cadieux, S.B., Brassell, S.C., Castañeda, I.S., Pratt, L.M. and White, J. (2015) Assessment of branched GDGTs as temperature proxies in sedimentary records from several small lakes in southwestern Greenland. *Organic Geochemistry*. **82**, 33-41.

Collinson, M., Hooker, J. and Grocke, D. (2003) Cobham lignite bed and penecontemporaneous macrofloras of southern England: A record of vegetation and fire across the Paleocene-Eocene Thermal Maximum. *Special Papers - Geological Society of American*, 333-350.

Collinson, M.E., Smith, S.Y., van Konijnenburg-van Cittert, J.H., Batten, D.J., van der Burgh, J., Barke, J. and Marone, F. (2013) New observations and synthesis of Paleogene heterosporous water ferns. *International Journal of Plant Sciences*.**174**, 350-363.

Collinson, M.E., Steart, D.C., Harrington, G.J., Hooker, J.J., Scott, A.C., Allen, L.O., Glasspool, I.J. and Gibbons, S.J. (2009) Palynological evidence of vegetation dynamics in response to palaeoenvironmental change across the onset of the Paleocene-Eocene Thermal Maximum at Cobham, Southern England. *Grana* **48**, 38-66.

Cox, P. M., Huntingford, C., and Harding, R. J. (1998) A canopy conductance and photosynthesis model for use in a GCM land surface scheme. *Journal of Hydrology*, **212–213**, 79–94.

Cox, P. M., Betts, R. A., Bunton, C. B., Essery, R. L. H., Rowntree, P. R., and Smith, J (1999) The impact of new land surface physics on the GCM simulation of climate and climate sensitivity. *Climate Dynamics*, **15**, 183–203.

Currano, E.D., Wilf, P., Wing, S.L., Labandeira, C.C., Lovelock, E.C. and Royer, D.L.. (2008) Sharply increased insect herbivory during the Paleocene–Eocene Thermal Maximum. *Proceedings of the National Academy of Sciences*. **105**, 1960-1964.

De Jonge, C., Hopmans, E.C., Zell, C.I., Kim, J.-H., Schouten, S. and Sinninghe Damsté, J.S. (2014) Occurrence and abundance of 6-methyl branched glycerol dialkyl glycerol tetraethers in soils: Implications for palaeoclimate reconstruction. *Geochimica et Cosmochimica Acta*, **141**, 97-112.

Dickson, A.J., Cohen, A.S., Coe, A.L., Davies, M., Shcherbinina, E.A. and Gavrilov, Y.O. (2015) Evidence for weathering and volcanism during the PETM from Arctic Ocean and Peri-Tethys osmium isotope records. *Palaeogeography, Palaeoclimatology, Palaeoecology*, **438**, 300-307.

Eldrett, J., Greenwood, D., Polling, M., Brinkhuis, H. and Sluijs, A. (2014) A seasonality trigger for carbon injection at the Paleocene–Eocene Thermal Maximum. *Climate of the Past*, **10**, 759-769.

Farnsworth, A., Lunt, D.J., O'Brien, C., Inglis, G.N., Foster, G.L., Markwick, P., Pancost, R.D and Robinson, S.A (2019) Climate sensitivity on geological timescales controlled by non-linear feedbacks and ocean circulation. *Geophysical Research Letters*. Accepted.

Fricke, H.C. and Wing, S.L. (2004) Oxygen isotope and paleobotanical estimates of temperature and $\delta^{18}O$–latitude gradients over North America during the early Eocene. *American Journal of Science*, **304**, 612-635.

Frieling, J., Gebhardt, H., Huber, M., Adekeye, O.A., Akande, S.O., Reichart, G.-J., Middelburg, J.J., Schouten, S. and Sluijs, A. (2017) Extreme warmth and heat-stressed plankton in the tropics during the Paleocene-Eocene Thermal Maximum. *Science Advances*, **3**, e1600891.

Frieling, J., Iakovleva, A.I., Reichart, G.-J., Aleksandrova, G.N., Gnibidenko, Z.N., Schouten, S. and Sluijs, A. (2014) Paleocene–Eocene warming and biotic response in the epicontinental West Siberian Sea. *Geology*, **42**, 767-770.

Garel, S., Schnyder, J., Jacob, J., Dupuis, C., Boussafir, M., Le Milbeau, C., Storme, J.-Y., Iakovleva, A.I., Yans, J., Baudin, F., Fléhoc, C. and Quesnel, F. (2013) Paleohydrological and paleoenvironmental changes recorded in terrestrial sediments of the Paleocene–Eocene boundary (Normandy, France). *Palaeogeography, Palaeoclimatology, Palaeoecology*, **376**, 184-199.

Gehler, A., Gingerich, P.D. and Pack, A. (2016) Temperature and atmospheric CO_2 concentration estimates through the PETM using triple oxygen isotope analysis of mammalian bioapatite. *Proceedings of the National Academy of Sciences* **113**, 7739-7744.

Gutjahr, M., Ridgwell, A., Sexton, P.F., Anagnostou, E., Pearson, P.N., Pälike, H., Norris, R.D., Thomas, E. and Foster, G.L. (2017) Very large release of mostly volcanic carbon during the Palaeocene–Eocene Thermal Maximum. *Nature*, **548**, 573-577

Handley, L., O'Halloran, A., Pearson, P.N., Hawkins, E., Nicholas, C.J., Schouten, S., McMillan, I.K. and Pancost, R.D. (2012) Changes in the hydrological cycle in tropical East Africa during the Paleocene–Eocene Thermal Maximum. *Palaeogeography, Palaeoclimatology, Palaeoecology*, **329**, 10-21.

Hollis, C.J., Dunkley Jones, T., Anagnostou, E., Bijl, P.K., Cramwinckel, M.J., Cui, Y., Dickens, G.R., Edgar, K.M., Eley, Y., Evans, D., Foster, G.L., Frieling, J., Inglis, G.N., Kennedy, E.M., Kozdon, R., Lauretano, V., Lear, C.H., Littler, K., Meckler, N., Naafs, B.D.A., Pälike, H., Pancost, R.D., Pearson, P., Royer, D.L., Salzmann, U., Schubert, B., Seebeck, H., Sluijs, A., Speijer, R., Stassen, P., Tierney, J., Tripati, A., Wade, B., Westerhold, T., Witkowski, C., Zachos, J.C., Zhang, Y.G., Huber, M. and Lunt, D.J. (2019) The DeepMIP contribution to PMIP4: methodologies for selection, compilation and analysis of latest Paleocene and early Eocene climate proxy data, incorporating version 0.1 of the DeepMIP database. *Geoscientific Model Development Discussion*. 1-98.

590 Hopmans, E.C., Schouten, S. and Sinninghe Damsté, J.S. (2016) The effect of
591 improved chromatography on GDGT-based palaeoproxies. *Organic*
592 *Geochemistry*, **93**, 1-6.
593 Huguet, A., Grossi, V., Belmahdi, I., Fosse, C. and Derenne, S. (2015) Archaeal and
594 bacterial tetraether lipids in tropical ponds with contrasting salinity
595 (Guadeloupe, French West Indies): Implications for tetraether-based
596 environmental proxies. *Organic Geochemistry*. **83**, 158-169.
597 Inglis, G.N., Collinson, M.E., Riegel, W., Wilde, V., Farnsworth, A., Lunt, D.J., Valdes,
598 P., Robson, B.E., Scott, A.C., Lenz, O.K., Naafs, B.D.A. and Pancost, R.D.
599 (2017) Mid-latitude continental temperatures through the early Eocene in
600 western Europe. *Earth and Planetary Science Letters,* **460**, 86-96.
601 Inglis, G.N., Naafs, B.D.A., Zheng, Y., McClymont, E.L., Evershed, R.P. and Pancost,
602 R.D. (2018) Distributions of geohopanoids in peat: Implications for the use of
603 hopanoid-based proxies in natural archives. *Geochimica et Cosmochimica*
604 *Acta*, **224**, 249-261.
605 Jaramillo, C., Ochoa, D., Contreras, L., Pagani, M., Carvajal-Ortiz, H., Pratt, L.M.,
606 Krishnan, S., Cardona, A., Romero, M., Quiroz, L., Rodriguez, G., Rueda, M.J.,
607 de la Parra, F., Morón, S., Green, W., Bayona, G., Montes, C., Quintero, O.,
608 Ramirez, R., Mora, G., Schouten, S., Bermudez, H., Navarrete, R., Parra, F.,
609 Alvarán, M., Osorno, J., Crowley, J.L., Valencia, V. and Vervoort, J. (2010)
610 Effects of Rapid Global Warming at the Paleocene-Eocene Boundary on
611 Neotropical Vegetation. *Science,* **330**, 957-961.
612 John, C.M., Bohaty, S.M., Zachos, J.C., Sluijs, A., Gibbs, S., Brinkhuis, H. and
613 Bralower, T. (2008) North American continental margin records of the
614 Paleocene-Eocene thermal maximum: Implications for global carbon and
615 hydrological cycling. *Paleoceanography*. **23**. PA2217
616 Jones, T.D., Lunt, D.J., Schmidt, D.N., Ridgwell, A., Sluijs, A., Valdes, P.J. and Maslin,
617 M.. (2013) Climate model and proxy data constraints on ocean warming across
618 the Paleocene–Eocene Thermal Maximum. *Earth Science Reviews.* **125,** 123-
619 145.
620 Kender, S., Stephenson, M.H., Riding, J.B., Leng, M.J., Knox, R.W.B., Peck, V.L.,
621 Kendrick, C.P., Ellis, M.A., Vane, C.H. and Jamieson, R. (2012) Marine and
622 terrestrial environmental changes in NW Europe preceding carbon release at
623 the Paleocene–Eocene transition. E*arth and Planetary Science Letters*, **353**,
624 108-120.
625 Kiehl, J.T. and Shields, C.A. (2013) Sensitivity of the Palaeocene–Eocene Thermal
626 Maximum climate to cloud properties. *Philosophical Transactions of the Royal*
627 *Society of London A: Mathematical, Physical and Engineering Sciences,* **371**,
628 20130093.
629 Lunt, D.J., Dunkley Jones, T., Heinemann, M., Huber, M., LeGrande, A., Winguth, A.,
630 Loptson, C., Marotzke, J., Roberts, C.D., Tindall, J., Valdes, P. and Winguth,
631 C. (2012) A model–data comparison for a multi-model ensemble of early
632 Eocene atmosphere–ocean simulations: EoMIP. *Climate of the Past*, **8**, 1717-
633 1736.
634 Lunt, D.J., Farnsworth, A., Loptson, C., Foster, G.L., Markwick, P., O'Brien, C.L.,
635 Pancost, R.D., Robinson, S.A. and Wrobel, N. (2016) Palaeogeographic
636 controls on climate and proxy interpretation. *Climate of the Past,* **12**, 1181-1198.
637 McInerney, F.A. and Wing, S.L. (2011) The Paleocene-Eocene Thermal Maximum: A
638 perturbation of carbon cycle, climate, and biosphere with implications for the
639 future. *Annual Review of Earth and Planetary Sciences,* **39**, 489-516.

Myhre, A., Thiede, J. and Firth, J. (1995) Shipboard Scientific Party, Initial Reports: sites 907–913, North Atlantic-Arctic Gateways. Proceedings, Initial Reports, Ocean Drilling Program 151.

Naafs, B.D.A., Inglis, G.N., Zheng, Y., Amesbury, M.J., Biester, H., Bindler, R., Blewett, J., Burrows, M.A., del Castillo Torres, D., Chambers, F.M., Cohen, A.D., Evershed, R.P., Feakins, S.J., Gałka, M., Gallego-Sala, A., Gandois, L., Gray, D.M., Hatcher, P.G., Honorio Coronado, E.N., Hughes, P.D.M., Huguet, A., Könönen, M., Laggoun-Défarge, F., Lähteenoja, O., Lamentowicz, M., Marchant, R., McClymont, E., Pontevedra-Pombal, X., Ponton, C., Pourmand, A., Rizzuti, A.M., Rochefort, L., Schellekens, J., De Vleeschouwer, F. and Pancost, R.D. (2017) Introducing global peat-specific temperature and pH calibrations based on brGDGT bacterial lipids. *Geochimica et Cosmochimica Acta*, **208**, 285-301.

Naafs, B., McCormick, D., Inglis, G. and Pancost, R.. (2018a) Archaeal and bacterial H-GDGTs are abundant in peat and their relative abundance is positively correlated with temperature. *Geochimica et Cosmochimica Acta*. **227**, 156-170.

Naafs, B.D.A., Rohrssen, M., Inglis, G.N., Lähteenoja, O., Feakins, S.J., Collinson, M.E., Kennedy, E.M., Singh, P.K., Singh, M.P., Lunt, D.J. and Pancost, R.D. (2018b). High temperatures in the terrestrial mid-latitudes during the early Palaeogene. *Nature Geoscience*, **11**, 766.

Naafs, B.D.A., Inglis, G.N., Blewett, J., McClymont, E.L., Lauretano, V., Xie, S., Evershed, R.P. and Pancost, R.D. (2019) The potential of biomarker proxies to trace climate, vegetation, and biogeochemical processes in peat: A review. *Global and Planetary Change*. **179**. 57-79

Pancost, R.D., Baas, M., van Geel, B. and Sinninghe Damsté, J.S. (2003) Response of an ombrotrophic bog to a regional climate event revealed by macrofossil, molecular and carbon isotopic data. *The Holocene*, **13**, 921-932.

Pancost, R.D., Steart, D.S., Handley, L., Collinson, M.E., Hooker, J.J., Scott, A.C., Grassineau, N.V. and Glasspool, I.J. (2007) Increased terrestrial methane cycling at the Palaeocene–Eocene thermal maximum. *Nature,* **449**, 332-335.

Ravizza, G., Norris, R., Blusztajn, J., Aubry, M (2001) An osmium isotope excursion associated with the late Paleocene thermal maximum: Evidence of intensified chemical weathering. *Paleoceanography,* **16**, 155-163.

Sachse, D., Billault, I., Bowen, G.J., Chikaraishi, Y., Dawson, T.E., Feakins, S.J., Freeman, K.H., Magill, C.R., McInerney, F.A., Van der Meer, M.T., Polissar, P., Robins, R.J., Sachs, J.P., Schmidt, H-L., Sessions, A.L., White, J.W.C., West, J.B. and Kahmen, A (2012) Molecular paleohydrology: interpreting the hydrogen-isotopic composition of lipid biomarkers from photosynthesizing organisms. *Annual Review of Earth and Planetary Sciences*. **40**. 221-249.

Sagoo, N., Valdes, P., Flecker, R. and Gregoire, L.J. (2013) The Early Eocene equable climate problem: can perturbations of climate model parameters identify possible solutions? *Philosophical Transactions of the Royal Society A: Mathematical, Physical and Engineering Sciences*. **371**.

Schmitz, B. and Pujalte, V. (2007) Abrupt increase in seasonal extreme precipitation at the Paleocene-Eocene boundary. *Geology,* **35**, 215-218.

Schoon, P.L., Heilmann-Clausen, C., Schultz, B.P., Sinninghe Damsté, J.S. and Schouten, S. (2015) Warming and environmental changes in the eastern North Sea Basin during the Palaeocene–Eocene Thermal Maximum as revealed by biomarker lipids*. Organic Geochemistry*, **78**, 79-88.

689 Schouten, S., Woltering, M., Rijpstra, W.I.C., Sluijs, A., Brinkhuis, H. and Sinninghe
690 Damsté, J.S. (2007) The Paleocene–Eocene carbon isotope excursion in
691 higher plant organic matter: Differential fractionation of angiosperms and
692 conifers in the Arctic. *Earth and Planetary Science Letters*, **258**, 581-592.
693 Secord, R., Bloch, J.I., Chester, S.G., Boyer, D.M., Wood, A.R., Wing, S.L., Kraus,
694 M.J., McInerney, F.A. and Krigbaum, J.J.S. (2012) Evolution of the earliest
695 horses driven by climate change in the Paleocene-Eocene Thermal Maximum.
696 *Science*, **335**, 959-962.
697 Secord, R., Gingerich, P.D., Lohmann, K.C. and MacLeod, K.G. (2010) Continental
698 warming preceding the Palaeocene-Eocene thermal maximum. *Nature*, **467**,
699 955-958.
700 Sinninghe Damsté, J.S.S., Rijpstra, W.I.C., Foesel, B.U., Huber, K.J., Overmann, J.,
701 Nakagawa, S., Kim, J.J., Dunfield, P.F., Dedysh, S.N. and Villanueva, (2018)
702 An overview of the occurrence of ether-and ester-linked iso-diabolic acid
703 membrane lipids in microbial cultures of the Acidobacteria: Implications for
704 brGDGT paleoproxies for temperature and pH. *Organic Geochemistry*. **124**, 63-
705 76.
706 Sluijs, A., Bijl, P., Schouten, S., Röhl, U., Reichart, G.-J. and Brinkhuis, H. (2011)
707 Southern ocean warming, sea level and hydrological change during the
708 Paleocene-Eocene thermal maximum. *Climate of the Past,* **7**, 47-61
709 Sluijs, A., Brinkhuis, H., Schouten, S., Bohaty, S.M., John, C.M., Zachos, J.C.,
710 Reichart, G.-J., Sinninghe Damsté, J.S., Crouch, E.M. and Dickens, G.R.
711 (2007) Environmental precursors to rapid light carbon injection at the
712 Palaeocene/Eocene boundary. *Nature,* **450**, 1218-1221.
713 Sluijs, A., Schouten, S., Pagani, M., Woltering, M., Brinkhuis, H., Sinninghe Damsté,
714 J.S., Dickens, G.R., Huber, M., Reichart, G.-J. and Stein, R. (2006) Subtropical
715 Arctic Ocean temperatures during the Palaeocene/Eocene thermal maximum.
716 *Nature* **441**, 610-613.
717 Sluijs, A., van Roij, L., Harrington, G.J., Schouten, S., Sessa, J.A., LeVay, L.J.,
718 Reichart, G.J. and Slomp, C.P. (2014) Warming, euxinia and sea level rise
719 during the Paleocene–Eocene Thermal Maximum on the Gulf Coastal Plain:
720 implications for ocean oxygenation and nutrient cycling. *Climate of the Past*. **10**,
721 1421-1439.
722 Smith, J.J., Hasiotis, S.T., Kraus, M.J. and Woody, D. (2009) Transient dwarfism of
723 soil fauna during the Paleocene–Eocene Thermal Maximum. *Proceedings of*
724 *the National Academy of Sciences,* **106**, 17655-17660.
725 Tierney, J.E., Russell, J.M., Eggermont, H., Hopmans, E., Verschuren, D. and
726 Sinninghe Damsté, J.S. (2010) Environmental controls on branched tetraether
727 lipid distributions in tropical East African lake sediments. *Geochimica et*
728 *Cosmochimica Acta*. **74**, 4902-4918.
729 Tierney, J.E. and Russell, J.M (2009) Distributions of branched GDGTs in a tropical
730 lake system: implications for lacustrine application of the MBT/CBT paleoproxy.
731 *Organic Geochemistry*. **40**, 1032-1036.
732 Tripati, A. and Elderfield, H. (2005) Deep-Sea Temperature and Circulation Changes
733 at the Paleocene-Eocene Thermal Maximum. *Science,* **308**, 1894-1898.
734 Valdes, P.J., Armstrong, E., Badger, M.P., Bradshaw, C.D., Bragg, F., Davies-
735 Barnard, T., Day, J.J., Farnsworth, A., Hopcroft, P.O., Kennedy, A.T. and Lord,
736 N.S. (2017). The BRIDGE HadCM3 family of climate models: HadCM3@ Bristol
737 v1. 0. *Geoscientific Model Development*, **10**, 3715-3743.

Weber, Y., Sinninghe Damsté, J.S., Zopfi, J., De Jonge, C., Gilli, A., Schubert, C.J., Lepori, F., Lehmann, M.F. and Niemann, H (2018) Redox-dependent niche differentiation provides evidence for multiple bacterial sources of glycerol tetraether lipids in lakes. *Proceedings of the National Academy of Sciences*. **115,** 10926-10931.

Weijers, J.W.H., Schouten, S., van der Linden, M., van Geel, B. and Sinninghe Damsté, J.S. (2004) Water table related variations in the abundance of intact archaeal membrane lipids in a Swedish peat bog. *FEMS Microbiology Letters*. **239**. 51-56.

Weijers, J.W., Schouten, S., van den Donker, J.C., Hopmans, E.C. and Sinninghe Damsté, J.S., (2007). Environmental controls on bacterial tetraether membrane lipid distribution in soils. *Geochimica et Cosmochimica Acta*, **71**, 703-713.

Weijers, J.W., Steinmann, P., Hopmans, E.C., Schouten, S. and Sinninghe Damsté, J.S. (2011) Bacterial tetraether membrane lipids in peat and coal: Testing the MBT–CBT temperature proxy for climate reconstruction. *Organic Geochemistry*, **42**, 477-486.

Wing, S.L., Harrington, G.J., Smith, F.A., Bloch, J.I., Boyer, D.M. and Freeman, K.H. (2005) Transient Floral Change and Rapid Global Warming at the Paleocene-Eocene Boundary. *Science,* **310,** 993-996.

Yang, H., Lü, X., Ding, W., Lei, Y., Dang, X. and Xie, S. (2015) The 6-methyl branched tetraethers significantly affect the performance of the methylation index (MBT′) in soils from an altitudinal transect at Mount Shennongjia. *Organic Geochemistry*. **82**, 42-53.

Zachos, J.C., Dickens, G.R. and Zeebe, R.E. (2008) An early Cenozoic perspective on greenhouse warming and carbon-cycle dynamics. *Nature,* **451**, 279-283.

Zachos, J.C., Schouten, S., Bohaty, S., Quattlebaum, T., Sluijs, A., Brinkhuis, H., Gibbs, S. and Bralower, T. (2006) Extreme warming of mid-latitude coastal ocean during the Paleocene-Eocene Thermal Maximum: Inferences from TEX_{86} and isotope data. *Geology* **34**, 737-740.

Zink, K.-G., Vandergoes, M.J., Mangelsdorf, K., Dieffenbacher-Krall, A.C. and Schwark (2010) Application of bacterial glycerol dialkyl glycerol tetraethers (GDGTs) to develop modern and past temperature estimates from New Zealand lakes. *Organic Geochemistry*. **41**, 1060-1066.

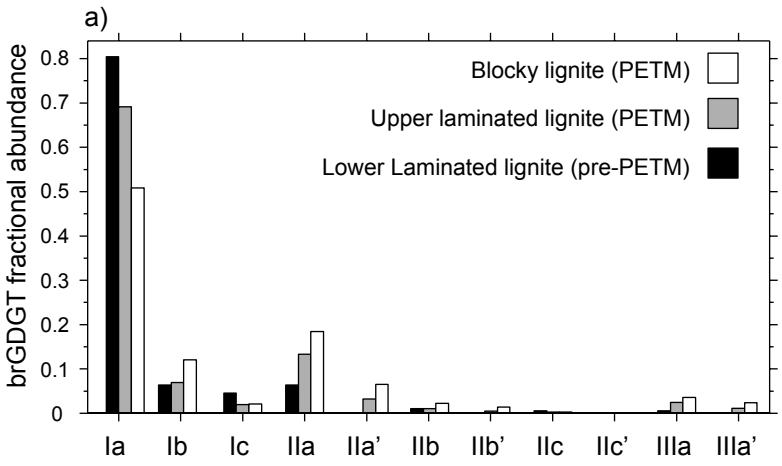
a)
brGDGT fractional abundance
0.8
0.7
0.6
0.5
0.4
0.3
0.2
0.1
0
Blocky lignite (PETM)
Upper laminated lignite (PETM)
Lower Laminated lignite (pre-PETM)
Ia
Ib
Ic
IIa
IIa'
IIb
IIb'
IIc
IIc'
IIIa
IIIa'

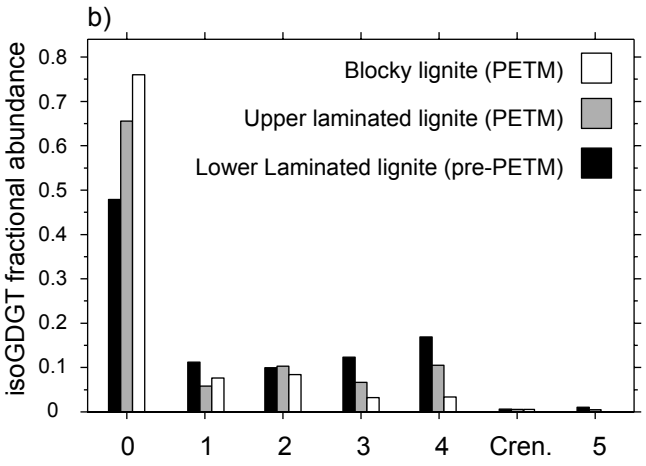
b)
isoGDGT fractional abundance
0.8
0.7
0.6
0.5
0.4
0.3
0.2
0.1
0
Blocky lignite (PETM)
Upper laminated lignite (PETM)
Lower Laminated lignite (pre-PETM)
0
1
2
3
4
Cren.
5

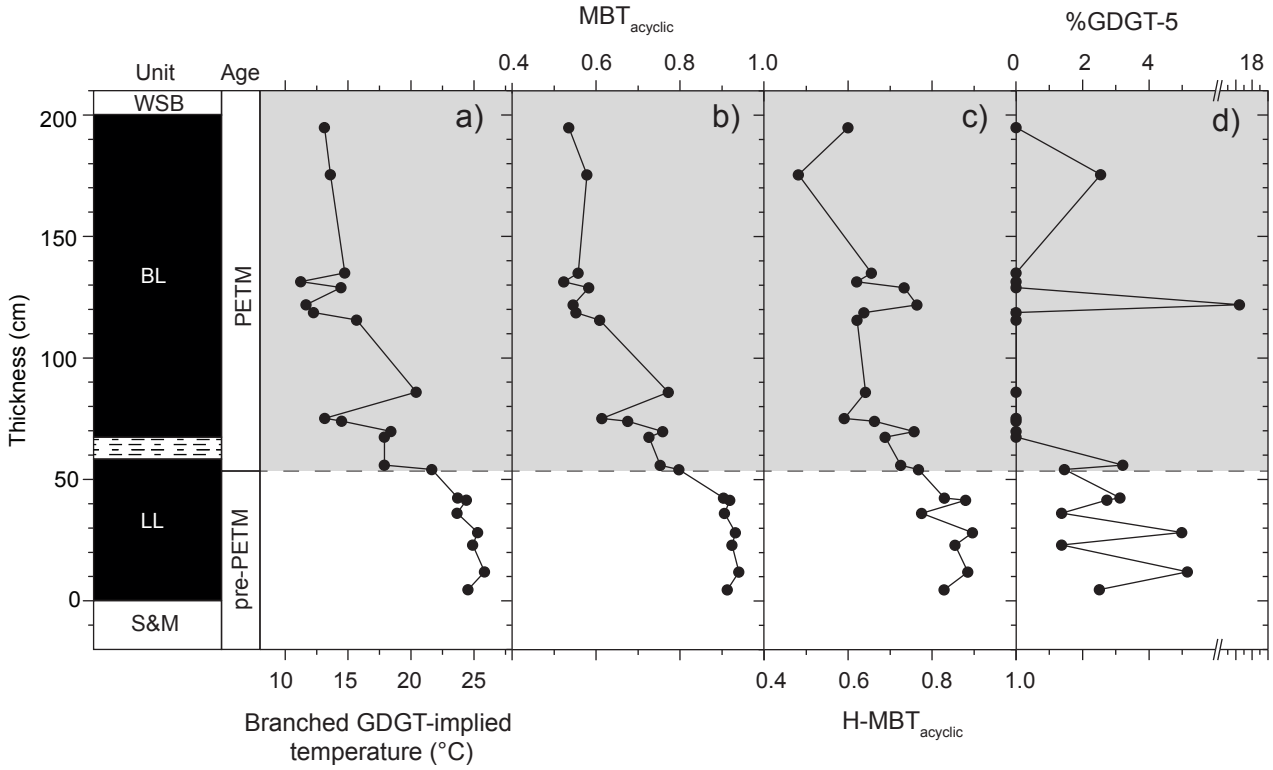
MBT acyclic
%GDGT-5
Unit
Age
WSB
BL
LL
S&M
PETM
pre-PETM
Thickness (cm)
a)
b)
c)
d)
Branched GDGT-implied temperature (°C)
H-MBT acyclic

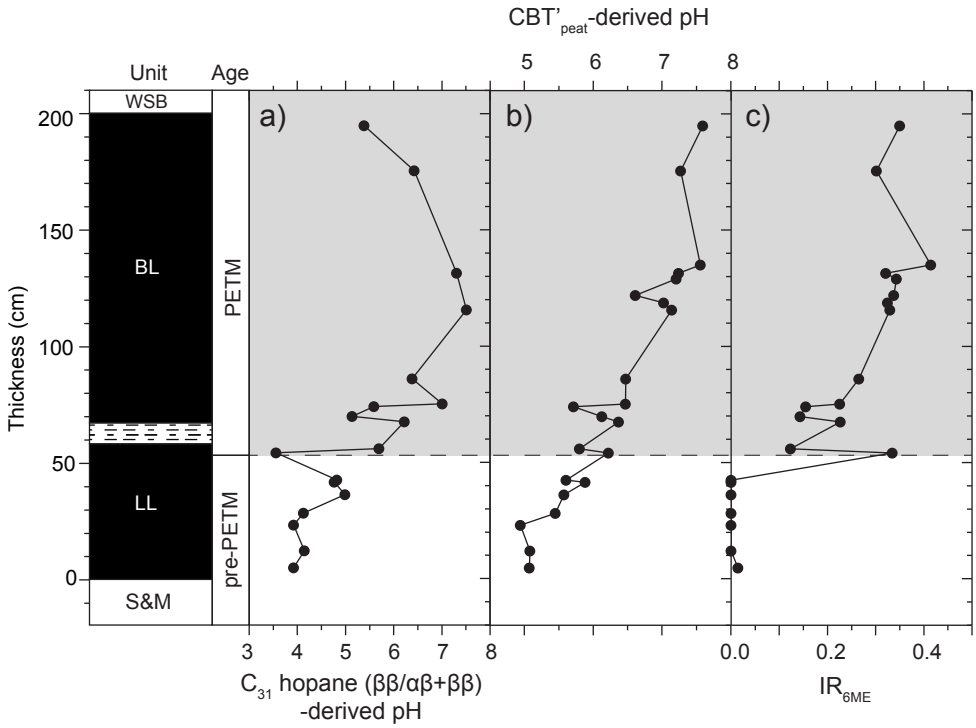
CBT'peat-derived pH
Unit
Age
WSB
BL
LL
S&M
PETM
pre-PETM
Thickness (cm)
a)
b)
c)
C31 hopane (ββ/αβ+ββ) -derived pH
IR6ME

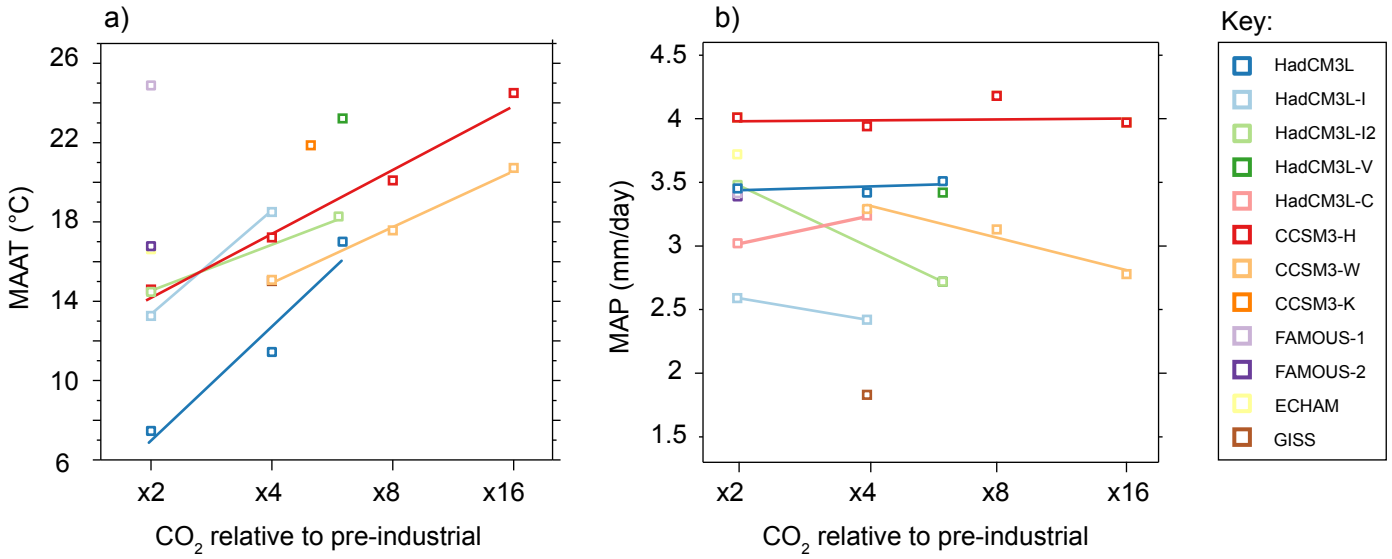
a)
MAAT (°C)
26
22
18
14
10
6
x2
x4
x8
x16
CO2 relative to pre-industrial
b)
MAP (mm/day)
4.5
4
3.5
3
2.5
2
1.5
x2
x4
x8
x16
CO2 relative to pre-industrial
Key:
HadCM3L
HadCM3L-I
HadCM3L-I2
HadCM3L-V
HadCM3L-C
CCSM3-H
CCSM3-W
CCSM3-K
FAMOUS-1
FAMOUS-2
ECHAM
GISS